JOURNAL OF SOLID STATE CHEMISTRY 113, 281–288 (1994)

Electronic Transport Phenomena of $La_{2/3+x}TiO_{3-\delta}$ ($x < 0.2$): Metal–Nonmetal Transition by Electron Doping

In-Seon Kim,[1] Tetsurō Nakamura, Yoshiyuki Inaguma, and Mitsuru Itoh[2]

Research Laboratory of Engineering Materials, Tokyo Institute of Technology, Nagatsuta 4259, Midori-ku, Yokohama 227, Japan

Received September 1, 1993; in revised form February 21, 1994; accepted February 23, 1994

Carriers were introduced into $La_{2/3}TiO_3$, an insulator with double perovskite structure having an *A*-site vacancy, by a hydrogen reduction, and their electronic transport phenomena and crystal structure were studied. The lightly doped samples showed semiconducting behavior, while the heavily doped samples showed metallic conductivity. This carrier-concentration-dependent metal–nonmetal transition has been found at 3*d* electron density of 0.33 per formula unit with simultaneous occurrence of a crystal symmetry change from *P4/mmm* to *Pnma*. The electronic state of the $La_{2/3+x}TiO_{3-\delta}$ system was characterized by measuring the resistivity, the Seebeck coefficient, and the magnetic susceptibility.

INTRODUCTION

For perovskite-type oxides with the general formula ABO_3, many *A*-site-deficient compounds have been reported. ReO_3 and WO_3 are the well-known examples of *A*-site-vacant perovskites; ReO_3 is known to have the highest conductivity among oxide conductors. When some cations are introduced into the vacant *A*-sites of the perovskites, *A*-site-deficient perovskites such as $Na_{1-x}WO_3$($0.05 \leq x \leq 0.70$) (1), $Sr_{1-x}NbO_3$($0.05 \leq x \leq 0.30$) (2), and $La_{1-x}TiO_3$($0.03 \leq x \leq 0.33$) (3) can be obtained. In the *A*-site-deficient perovskite $La_{1/3}NbO_3$, two-thirds of the *A*-sites are vacant. In this case, the La ion and the vacancy settle into an ordered arrangement, resulting in a double perovskite structure with a doubled periodicity along the *c* axis $c = 2a$. $La_{1/3}MO_3$, $Ce_{1/3}MO_3$, $Nd_{1/3}MO_3$(*M* = Nb, Ta), and $Ln_{1/3}TaO_3$ (*Ln* = Gd, Dy, Y, Yb, Ho, Er) are reported to have the double perovskite structure (4, 5). In the crystal structure of $La_{1/3}NbO_3$, there are two NbO_6 octahedra in the unit cell. The ordered arrangement of the La ion and the vacancy in the *A*-site stabilize the displacement of Nb ion along the *c* axis from the center of the octahedra such that the O–Nb–O bond angle in the *c* plane is 163° in the NbO_6 octahedra (5).

The crystal structure of $La_{2/3}TiO_3$ (6) with one-third of the *A*-sites cation vacant was reported to be the same as that of $La_{1/3}NbO_3$ (6). The dielectric properties of the solid solution system $La_{2/3}TiO_3$–$SrTiO_3$ have been reported (7, 8), but detailed properties of $La_{2/3}TiO_3$ have not yet been published. Since Ti ions shift from the center of the TiO_6 octahedra in the double perovskite $La_{2/3}TiO_3$, quasi-two-dimensional properties are expected in this compound, due to the ordered arrangement in the *A*-site. The orthorhombic *Pmmm* (No. 47) structure of $La_{2/3}TiO_3$ is shown in Fig. 1.

In this report, the electrical conductivity and crystal structure of electron-introduced $La_{2/3}TiO_3$ double perovskite were investigated. We varied the 3*d* electron density in the range 0 to 0.6 per formula unit by introducing oxygen vacancies and by substituting La into an *A*-site vacancy in $La_{2/3+x}TiO_{3-\delta}$; we discuss the crystal structure, electrical conductivity, and magnetic properties of the $La_{2/3+x}TiO_{3-\delta}$ system as a function of carrier density.

EXPERIMENTAL

The oxygen-deficient compounds $La_{2/3+x}TiO_{3-\delta}$ ($0 \leq x \leq 0.2$) were synthesized by the conventional solid-state reaction method. The required amounts of La_2O_3 (99.99%) and TiO_2 (99.9%) were mixed in an agate mortar with ethanol. The amount of metal ion in La_2O_3 was determined by EDTA. The mixed powder was fired at 1423 K for 72 hr under flowing hydrogen gas with several intermediate grindings. The ground powder was pressed into pellets, placed in a tungsten crucible, and fired at 1673–1973 K for about 6 hr with intermittent grinding. An electric furnace with a tungsten heating element was evacuated and filled with dry hydrogen gas passed through a liquid-nitrogen trap. Reducing conditions for the desired oxygen deficiency δ up to ~0.2 were chosen by changing the heating temperature from 1173 to 1973 K. The temperature was measured by a W–5%Re/W–26%Re thermocouple. After reduction, the samples were quenched to room tempera-

[1] Present address: Superconductivity Laboratory, Korea Research Institute of Standards and Science, P.O. Box 3, Taedok Science Town, Taejon, Korea.

[2] To whom correspondence should be addressed.

0022-4596/94 $6.00

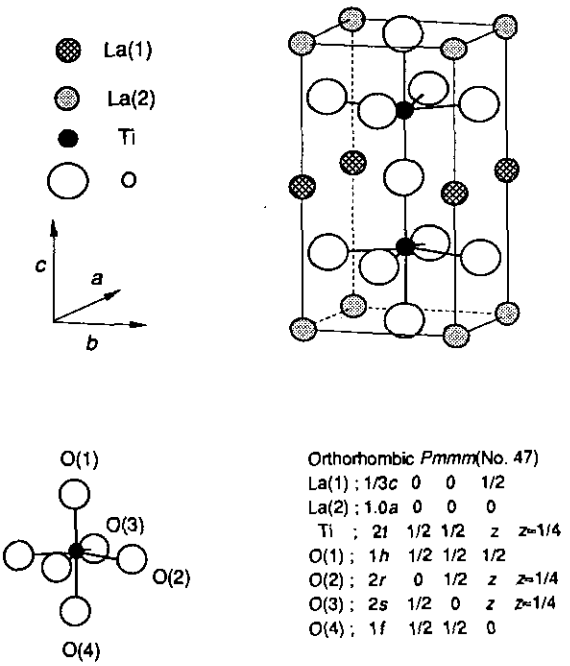

FIG. 1. Crystal structure of the double perovskite $La_{2/3}TiO_3$.

ture under hydrogen gas. The oxygen vacancy δ was determined by thermogravimetry, and the carrier density was calculated by invoking charge neutrality, supposing one oxygen vacancy to provide two electrons to the Ti ion.

Lattice parameters were obtained by least-squares fitting of diffraction lines taken on a Rigaku X-ray diffractometer, with Si powder as an internal standard. Diffraction data were collected at higher 2θ angles (80–120°) to distinguish Cu$K\alpha_1$ lines from Cu$K\alpha_2$ lines. The powder X-ray Rietveld analysis was carried out for 5000 diffractions, which were recorded by a MAC Science X-ray diffractometer using graphite monochromated Cu$K\alpha$ radiation. The data were taken from 20° to 120° (2θ) with a 0.02° step scan.

The resistivity was measured from room temperature down to 10 K by a standard four-probe method. Silver wire (0.1 mm ϕ) leads were attached to the bar-shaped samples. Thermoelectric data were obtained for the bar-shaped samples using two gold point contacts, which were welded by two chromel–constantan thermocouples, respectively. The residual thermal emf was calibrated with platinum and nickel, whose Seeback coefficients are accurately known (9–11). DC magnetic susceptibility measurements were made by a SQUID magnetometer (Quantum Design MPMS2) over the temperature range 5 to 300 K at a constant magnetic field of 1 T.

RESULTS AND DISCUSSIONS

Crystal structures. It is known that the crystal structure of $La_{2/3}TiO_{3-\delta}$ changes as a function of the oxygen deficiency δ and temperature. Figure 2 shows the temperature dependence of the dielectric constant for $La_{2/3}TiO_3$ measured in the range 1 kHz–10 MHz. In this frequency range, the dielectric constant (with dielectric loss <0.001) was found to be almost constant and relaxation was not observed. This material is an insulator with a high but almost temperature-independent dielectric constant. Abe and Uchino (6) reported the δ dependence of the phase transition of $La_{2/3}TiO_{3-\delta}$: with increasing δ the structure changes from an orthorhombic double perovskite to a tetragonal double perovskite and to a cubic perovskite at $\delta = 0.024$ and at $\delta = 0.046$, respectively. The X-ray diffraction patterns of $La_{2/3}TiO_{2.970}$ and $La_{2/3}TiO_{2.870}$ samples in the present experiment exhibit the orthorhombic and tetragonal structures of the double perovskite, respectively, as shown in Fig. 3. Iyer and Smith (5) determined the crystal structure of $La_{1/3}TaO_3$ to be the space group $P4/mmm$ to which $La_{2/3}TiO_3$ belongs. We carried out the powder X-ray Rietveld analysis by the RIETAN program (12, 13), applying the space group $Pmmm$ for orthorhombic $La_{2/3}TiO_{2.970}$, and the space group $P4/mmm$ for tetragonal $La_{2/3}TiO_{2.870}$, respectively. In this study, we could observe weak superlattice lines deriving from the double perovskite even for very strongly reduced samples such as $La_{2/3}TiO_{2.835}$ ($\delta = 0.165$), showing that a cubic phase does not appear even at this vacancy density. The results of Rietveld profile refinement for $La_{2/3}TiO_{2.835}$ gave rise to slightly different occupation factors between the La(1)-site and the La(2)-site, as shown in Tables 1a and 1b. It is considered that the crystal symmetry of $La_{2/3}TiO_{3-\delta}$ is not subject to change from the tetragonal to the cubic structure at room temperature upon variation of oxygen deficiency up to $\delta = 0.165$, which is the highest value of δ obtainable in our experiment. The crystal symmetry showed a transition from tetragonal double perovskite to

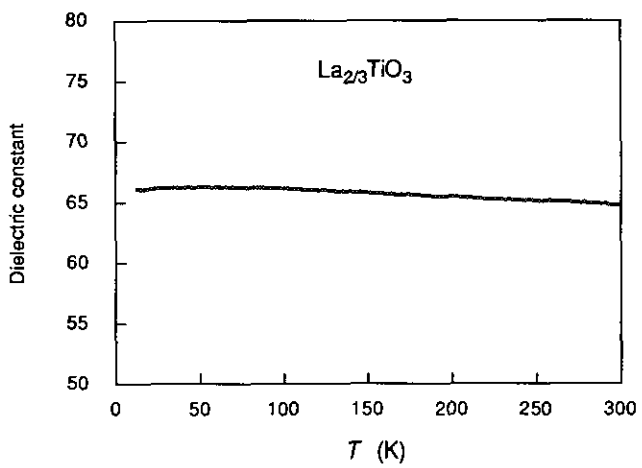

FIG. 2. Temperature dependence of the dielectric constant measured for $La_{2/3}TiO_3$.

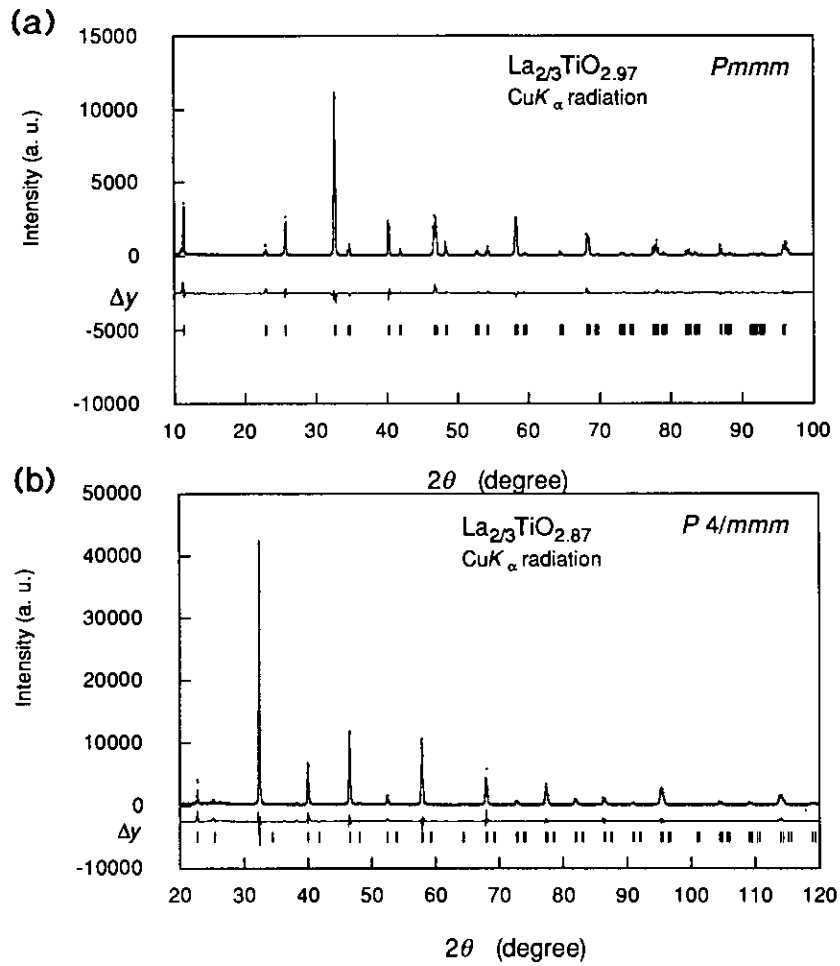

FIG. 3. Observed, calculated, and difference powder X-ray diffraction profiles of (a) orthorhombic $La_{2/3}TiO_{2.970}$ and (b) tetragonal $La_{2/3}TiO_{2.870}$.

an orthorhombic $GdFeO_3$ type when the carrier density was increased by introduction of La into the *A*-site vacancy. The transition occurred at $y \approx 0.33$, where the y value is the ratio of Ti^{3+} ion to the total titanium ion, calculated from the amount of oxygen deficiency based on invoking charge neutrality for $La_{2/3+x}Ti^{3+}_{y}Ti^{4+}_{1-y}O_{3-\delta}$. The lattice parameters of the solid solution system are shown in Fig. 4 as a function of y, where a_0, b_0, and c_0 represent the lattice constants for unit formula. The crystal structure changes from orthorhombic *Pmmm* to tetragonal *P4/mmm* at $y = 0.092$, and from the tetragonal to orthorhombic *Pnma* at $y = 0.33$. The lattice constants for $y = 0.092$ and 0.978 in Fig. 4 were taken from Ref. (6) and from the single crystal data of Ref. (14).

Resistivity. The resistivity of $La_{2/3}TiO_{2.981}$ and $La_{0.716}TiO_{2.928}$ samples is shown as a function of temperature in Fig. 5a, where the y values of these samples are 0.038 and 0.294, respectively. A negative slope in resistivity vs temperature is seen below room temperature for $y = 0.030$, but the slope turns positive for $y = 0.294$ below 70 K. The number of current carriers is generated as a function of temperature, i.e., is proportional to $\exp(-(E_C - E_F)/kT)$, where E_C is the conduction band level. When conduction occurs in a conduction band, a metallic temperature-dependent conductivity is anticipated, and $d\rho/dT$ has a positive value according to this relation. Thus, a slope in resistivity vs temperature could give us a rough guide for distinguishing the metalliclike or the semiconductive behavior. As shown in Fig. 5a, this type of metal–nonmetal transition versus temperature variation could be observed even in the heavily doped samples. In Fig. 5b, the resistivity data of $La_{2/3}TiO_{2.852}$ ($y = 0.296$), $La_{4/5}TiO_{2.976}$ ($y = 0.448$), and $La_{5/6}TiO_{2.982}$ ($y = 0.536$) are shown. The resistivity of the latter two samples showed an almost linear temperature dependence in the whole temperature range measured. The composition-dependent metal–nonmetal transition could be observed around $y \approx 0.33$ in the $La_{2/3+x}TiO_{3-\delta}$ system. This y value coincides with the y value where the phase transition occurs from *P4/mmm* to *Pnma*, as shown in Fig. 4. Figure 6a shows room-temperature resistivity vs y for the $La_{2/3+x}Ti^{3+}_{y}Ti^{4+}_{1-y}O_{3-\delta}$ system. The closed and hatched cir-

TABLE 1a
Crystal Data for Orthorhombic $La_{2/3}TiO_{2.970}$ and Tetragonal $La_{2/3}TiO_{2.870}$

Empirical formula	$La_{2/3}TiO_{2.970}$	$La_{2/3}TiO_{2.870}$
Crystal system	Orthorhombic	Tetragonal
Space group	*Pmmm* No. 47	*P4/mmm* No. 123
Cell constant	a = 3.8789(2) Å	a = 3.8980(3) Å
	b = 3.8668(2) Å	
	c = 7.7866(3) Å	c = 7.7949(10) Å
Z	2	2
Density	5.36 g/cm^3	5.25 g/cm^3
Radiation	Graphite monochromated Cu$K\alpha$	Graphite monochromated Cu$K\alpha$
2θ range	20–120°	20–120°
No. of data points	5000	5000
Reflections	256	154
Parameters for refinement	58	43
R factors (%)		
R_{wp}	17.7	14.2
R_p	13.3	11.0
R_e	8.0	4.8
R_i	8.5	3.8
R_f	7.8	3.9

cles respectively represent the data by MacLean *et al.* (15) and Lichtenberg *et al.* (16) in the oxygen-excess $LaTiO_{3+\delta}$ system. This figure shows the presence of the resistivity minimum around $y \approx 0.6$–0.7. In this region $y > 0.8$, a semiconducting behavior has been reported with an increase of y (15). In Fig. 6b we show the calculated mobility using the equation $\sigma = ne\mu$, where σ is conductivity, n is charge-density, and μ is mobility of the charge carriers, from the room-temperature resistivity data as shown in Fig. 6a. In the semiconductive region below $y \approx 0.33$, the mobility has values of order 10^{-2} cm^2/V sec, while in the metallic region it has values of order 1 cm^2/V sec. The mobility crosses 0.1 cm^2/V sec in the vicinity of $y \approx 0.33$, which is consistent with the value of $\mu = 0.1$ cm^2/V sec frequently adopted to distinguish an insulator from a metal (17). As shown in Fig. 6b the mobility seems to be saturated at about 1 cm^2/V sec even in the heavily doped samples. It is reported that $\mu = 0.1$ to 10 cm^2/V sec for cation–cation hopping (transfer of t_{2g} electrons between octahedral-site cations), and $\mu < 1$ cm^2/V sec indicates d electron charge carriers (18). The metal–nonmetal transition for the samples around $y \approx 0.33$ may be correlated to a Ti^{3+} ordering among the pseudo-two-dimensional double perovskite structure. A broad metal–nonmetal transition versus temperature in Fig. 5 may derive from some order–disorder transition of oxygen vacancies or overlapping of donor levels and a conduction band due to a rise in donor level with decreasing temperature, which is used to explain the metal–nonmetal transition in EuO (19).

Seebeck coefficient. Figure 7 shows the measured Seebeck coefficient $S(T)$ as a function of temperature for the samples with $y \leq 0.63$. $S(T)$ shows a metal-like linear dependence on T from 80 to ≈300 K with a negative absolute value. The sign of $S(T)$ establishes that the charge carriers are electrons. The Seebeck coefficient is expressed by (20, 21)

$$S = -\frac{\pi^2}{3}\frac{k_B}{e}k_B T\left(\frac{\partial \ln \Lambda}{\partial E} + \frac{\partial \ln B}{\partial E}\right)_{E=E_F}. \quad [1]$$

Here, Λ is the mean free path of electrons (charge $-e$), B is the area of the Fermi surface, and E is the electron energy. For a spherical band and single carrier formalism

TABLE 1b
Atomic Positional Parameters of Orthorhombic $La_{2/3}TiO_{2.970}$ and Tetragonal $La_{2/3}TiO_{2.870}$

Orthorhombic $La_{2/3}TiO_{2.970}$ (S.G. *Pmmm*)

Atom	Occupation	x	y	z	B_{eq}(Å^2)
La(1)	0.353(11)	0	0	1/2	0.49(40)
La(2)	0.981(11)	0	0	0	0.67(17)
Ti	1	1/2	1/2	0.2594(17)	1.08(23)
O(1)	1	1/2	1/2	1/2	1.54(1.66)
O(2)	1	0	1/2	0.2307(85)	1.10(1.73)
O(3)	1	1/2	0	0.2412(78)	0.23(1.31)
O(4)	1	1/2	1/2	0	1.96(1.78)

Bond distances (Å)

Ti–O(1)	1.8732(129)	Ti–O(4)	2.02021(129)
Ti–O(2)	1.9523(78)	La(1)–Ti	3.3179(73)
Ti–O(3)	1.9386(44)	La(2)–Ti	3.4030(77)

Bond angles

O(2)–Ti–O(2)	166.8°(4.0)	O(3)–Ti–O(3)	171.6°(3.6)

Tetragonal $La_{2/3}TiO_{2.870}$ (S. G. *P4/mmm*)

Atom	Occupation	x	y	z	B_{eq}(Å^2)
La(1)	0.616(60)	0	0	1/2	0.29(0.97)
La(2)	0.717(11)	0	0	0	0.39(0.85)
Ti	1	1/2	1/2	0.2547(109)	1.03(0.27)
O(1)	1	0	1/2	0.2330(269)	2.2(11.5)
O(2)	1	1/2	1/2	0	2.0(23.3)
O(3)	1	1/2	1/2	1/2	2.4(23.1)

Bond distances (Å)

Ti–O(1)	1.9558(97)	Ti–O(2)	1.9878(857)	Ti–O(3)	1.9089(857)

Bond angles

O(2)–Ti–O(2)	170.54°(6.9)

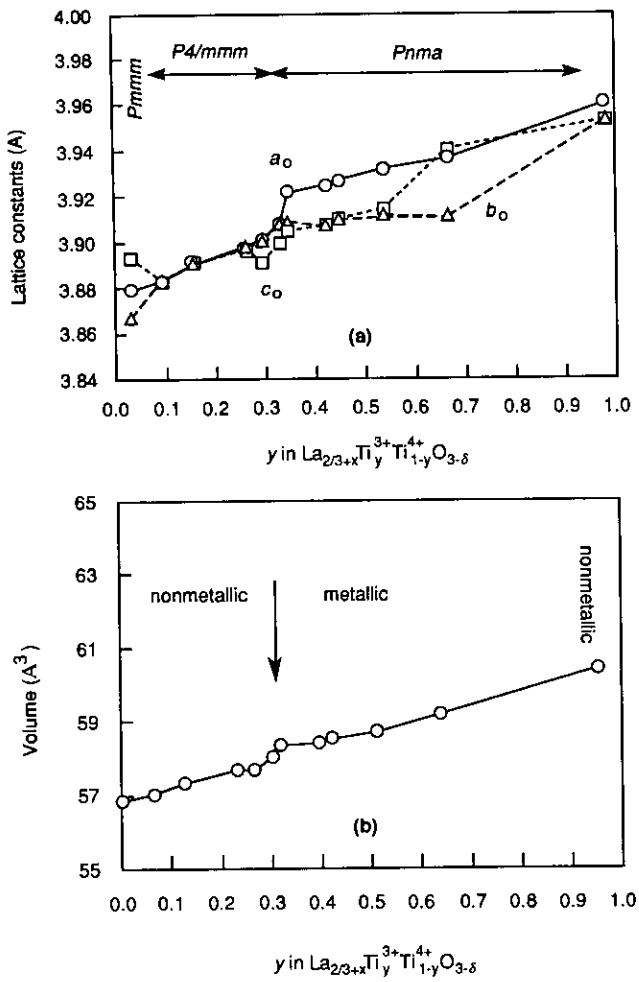

FIG. 4. Variations of the lattice parameters (a) and unit perovskite volume (b) with the concentration y of Ti^{3+} in the $La_{2/3+x}Ti^{3+}_yTi^{4+}_{1-y}O_{3-\delta}$ system. Data for $y = 0.092$ and 0.978 were taken from Refs. (6) and (14), respectively.

$(\partial \ln B/\partial E)_{E=E_F} = E_F^{-1}$. Then the equation for S reduces to the simple form

$$S = A\frac{\pi^2 k_B^2 T}{3eE_F}, \qquad [2]$$

where A is a parameter accounting for the contribution $\partial \ln \Lambda/\partial E$ with the constraints $1 \leq A \leq 3$. The slope $\partial S/\partial T$ gives the E_F. The E_F values calculated by using Eq. [2] are shown in Fig. 8 as a function of y. E_F increases linearly with increasing y up to $y \approx 0.33$. Above $y \approx 0.33$, E_F keeps a constant value of 0.27 eV. In perovskite-type oxides, the Fermi energy is reported to be 0.21 eV for $LaNiO_3$, 0.12 eV for $YBa_2Cu_3O_7$ (22), and 0.26 eV for La_2CuO_4 (23). The results from Fig. 8 suggest that E_F lies between the bottom of the empty conduction band and the Ti^{3+} donor level. With increasing y, E_F increases until it crosses the bottom of the conduction band and then the top of the donor level. When the crossing occurs, E_F no longer increases as a function of the carrier concentration; carriers (electrons) are accommodated in the presumably parabolic band and metallic behavior appears.

Magnetic properties. The temperature dependence of the magnetic susceptibility of $La_{2/3}TiO_{2.870}$, $La_{2/3}TiO_{2.835}$, $La_{0.767}TiO_{2.977}$, $La_{0.767}TiO_{2.93}$, and $La_{0.8}TiO_{2.976}$ samples is shown in Fig. 9. In the case of $La_{2/3}TiO_{2.870}$, the magnetic susceptibility increased with decreasing temperature at low temperature. The data were fitted to the Curie–Weiss law with a temperature-independent term, χ_{TIP}, following the equation

$$\chi = C/(T - \Theta) + \chi_{TIP}. \qquad [3]$$

From a fit to Eq. [3], we obtained a Curie constant of $C = 0.00289(1)$ emu K/mole ($p_{eff} = 0.152$), $\theta = -2.76(7)$ K, and $\chi_{TIP} = 27.3(2) \times 16^{-6}$ emu/mole for this sample. The other samples exhibited temperature-independent Pauli paramagnetism. In general, the paramagnetic susceptibility can be represented by the equation

$$\chi = \chi^{core} + \chi^{Pauli} + \chi^{Landau} + \chi^{Orbital}. \qquad [4]$$

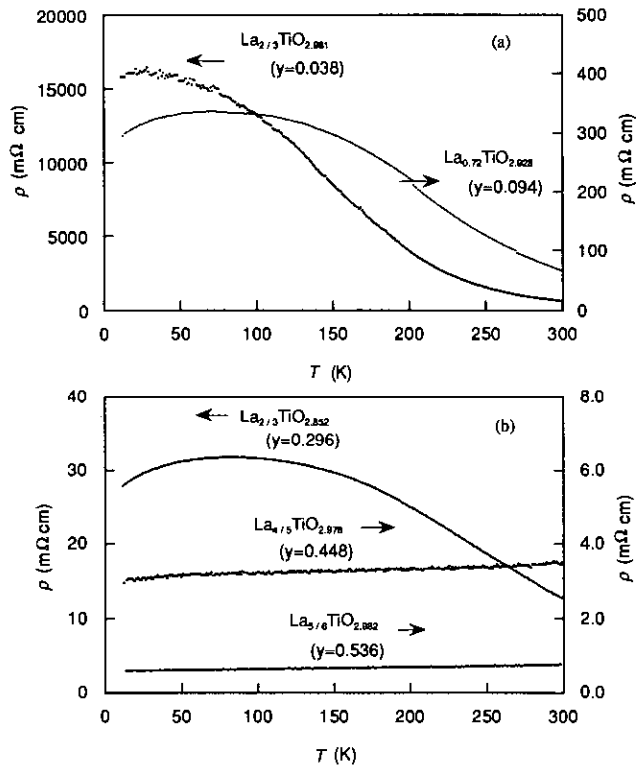

FIG. 5. Temperature dependencies of resistivities for the lightly doped (a) and heavily doped (b) $La_{2/3+x}TiO_{3-\delta}$.

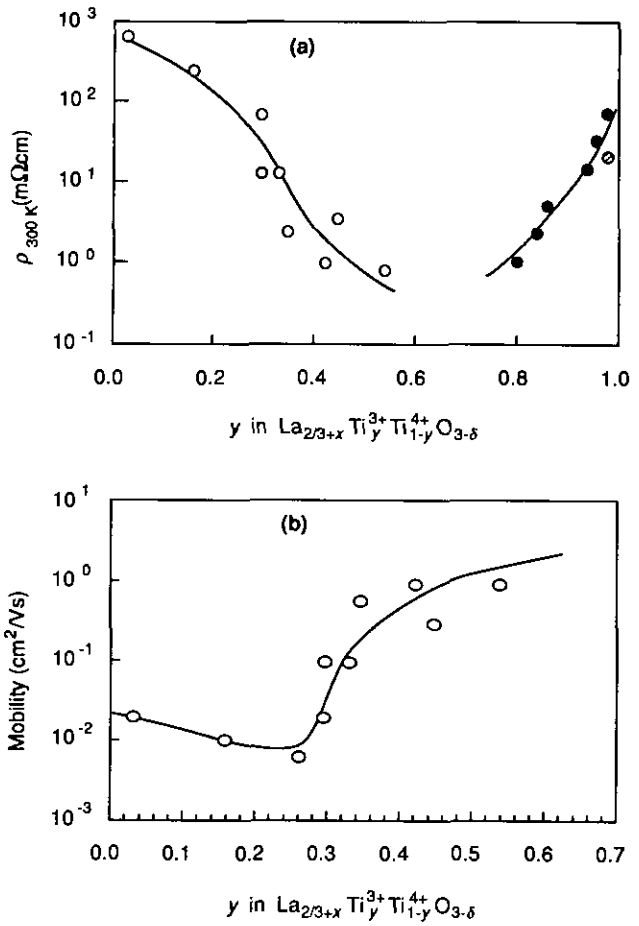

FIG. 6. (a) Room-temperature resistivity vs y in the $La_{2/3+x}Ti^{3+}_{y}Ti^{4+}_{1-y}O_{3-\delta}$ system. (Hatched and closed circles are from Refs. (15) and (16), respectively.) (b) Mobility vs y calculated from the room-temperature resistivity data. (The solid line in the figure is drawn as a visual guide.)

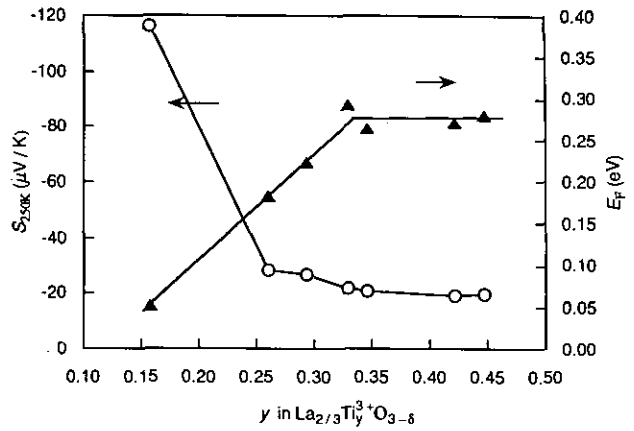

FIG. 8. Variation of the Seebeck coefficient at 250 K, and the Fermi energy with y in the $La_{2/3+x}Ti^{3+}_{y}Ti^{4+}_{1-y}O_{3-\delta}$ system.

Here, χ^{core} is the sum of the core diamagnetism and Van Vleck diamagnetism, χ^{Pauli} is the Pauli paramagnetism, χ^{Landau} is the Landau paramagnetic susceptibility, and $\chi^{Orbital}$ is the orbital contribution of susceptibility. The first term in Eq. [4] is due to the ion cores, and the last three terms are due to the conduction electrons. The diamagnetic contribution due to the Ti^{4+} core can be estimated to be 28×10^{-6} emu/mole from the published diamagnetic data and from the Van Vleck susceptibility (24–26). The electron Pauli paramagnetic susceptibility in the band structure can be expressed as

$$\chi^{Pauli} = (m^*/m)\chi_e^{Pauli} = \mu_B^2 N_{bs}(0), \qquad [5]$$

where χ_e^{Pauli} is the free electron Pauli paramagnetism ($= 3N\mu^2/2E_F$; Ref. (27)), μ_B is the Bohr magneton, $N_{bs}(0)$

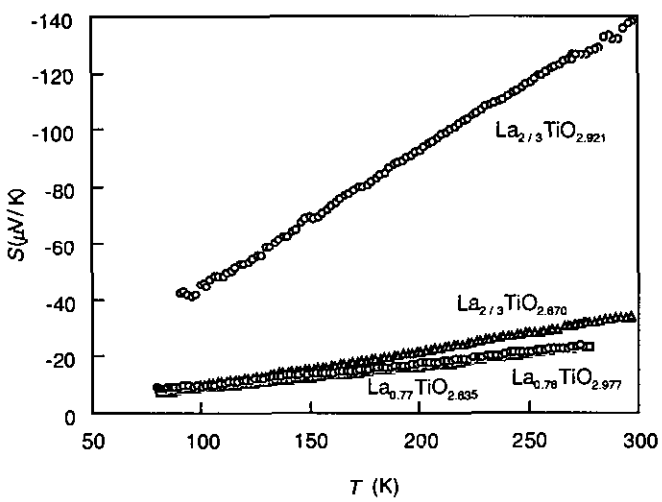

FIG. 7. Variation of the Seebeck coefficient S with the temperature of the $La_{2/3+x}TiO_{3-\delta}$ system.

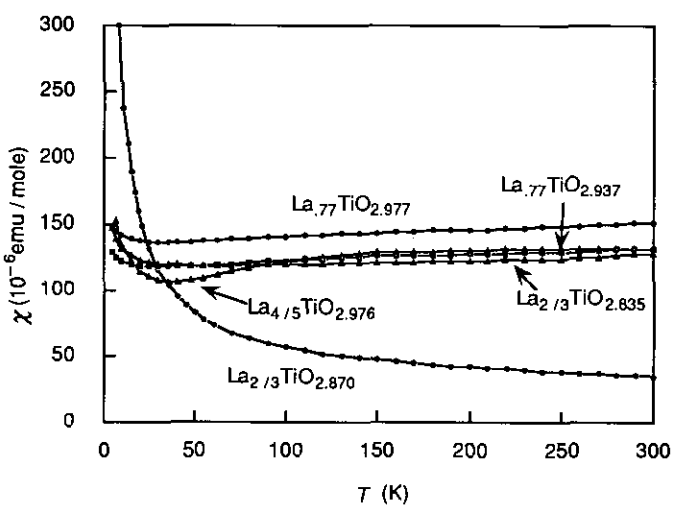

FIG. 9. Temperature dependence of the magnetic susceptibility of the $La_{2/3+x}TiO_{3-\delta}$ system.

TABLE 2
Electronic Parameters Characterizing the Conduction Electrons in $La_{2/3+x}Ti_y^{3+}Ti_{1-y}^{4+}O_{3-\delta}$ Derived from Magnetic Susceptibility Measurements

y (Ti^{3+} concn)	n (10^{21} cm^{-3})	χ_M (10^{-6} emu/mole)	χ_e^{Pauli} (10^{-6} emu/mole)	m^*/m	$N(0)$ states/eV-atom
0.260	4.39	27.3	12.9	2.3	0.20
0.330	5.54	134.9	14.0	9.7	0.93
0.346	5.78	141.9	14.3	9.9	0.93
0.426	7.11	161.9	15.3	10.6	1.07
0.448	7.50	123.1	15.6	7.9	0.80
$LiTi_2O_4$[a]	13.5	220	23.5	9.4	0.97
$YBa_2Cu_3O_7$[b]				9.6	
$LaNiO_3$[b]				11	
La_4CuO_4[c]				9 ~ 12	
Cu[b]				1.3	

[a] Ref. (28).
[b] Ref. (22).
[c] Ref. (23), effective mass of holes below 60 K.

is the density of electron energy states, m^* is the effective mass, and m is the electron mass. We used the relation $\chi^{Landau} = -(m/3m^*)\chi_e^{Pauli}$ as predicted in Ref. (28) and in the references therein, and we neglected the unknown orbital contribution. The temperature-independent Pauli paramagnetic susceptibility can then be expressed as

$$\chi = [(m^*/m) - (m/3m^*)]\chi^{Pauli} + \chi^{Core}. \quad [6]$$

This equation can be used for the effective mass calculation of conduction electrons from the measured susceptibility data. The calculated effective masses for $La_{2/3+x}Ti_y^{3+}Ti_{1-y}^{4+}O_{3-\delta}$ and other parameters are shown in Table 2. One obtains an effective mass of 2.3 for the $y = 0.26$ sample, and the effective mass ratio approaches 10 for the samples with $y \geq 0.33$, as shown in Table 2. It is characteristic of the Mott–Hubbard type metal–nonmetal transition, i.e., of the semiconductive–metallic transition and of the Curie–Weiss type–Pauli paramagnetic type transition accompanied by the increase of the effective mass with increasing y, that this change reflects the change in the electronic states of $La_{2/3+x}TiO_{3-\delta}$ from atomic to Bloch states. The $3d^1$ electrons are at donor levels below the conduction band when the concentration of doped carriers is small. The donor level overlaps with the bottom of the vacant conduction band to exhibit metallic conductivity when the amount of Ti^{3+} with its larger ionic radius and doped carrier concentration increases; this is accompanied by a change in the crystal symmetry from tetragonal to orthorhombic.

CONCLUSION

The crystal structure of the $La_{2/3}TiO_{3-\delta}$ system is orthorhombic $Pmmm$ in $\delta \leq 0.046$ and tetragonal $P4/mmm$ in $0.046 \leq \delta \leq 0.16$. In the $La_{2/3+x}Ti_y^{3+}Ti_{1-y}^{4+}O_{3-\delta}$ system, tetragonal $P4/mmm$ and orthorhombic $Pnma$ structures appear in the regions $y < 0.33$ and $y \geq 0.33$, respectively. The electrical resistivity of the $La_{2/3+x}Ti_y^{3+}Ti_{1-y}^{4+}O_{3-\delta}$ system shows semiconductive and metallic temperature dependencies around room temperature in the ranges $y < 0.33$ and $y \geq 0.33$, respectively. Semiconducting samples show metallic behavior at lower temperatures. The metal–nonmetal transition with temperature derives from overlapping of the vacant conduction band and the Ti^{3+} donor level. The metal–nonmetal transition close to $y \approx 0.33$ may be caused by the rise in the donor level, which then overlaps with the conduction band. The results of Seebeck coefficient measurements support the rise in the Fermi level. Magnetic susceptibility measurement revealed that Curie–Weiss-like paramagnetism and Pauli paramagnetism appear in the ranges $y < 0.3$ and $y \geq 0.33$, respectively. In the vicinity of $y \approx 0.33$, the effective mass of the conduction electrons increases from 2 to 10, which is characteristic of the Mott–Hubbard type metal–nonmetal transition.

ACKNOWLEDGMENT

The authors express their thanks for a Grant-in-Aid for Scientific Research from the Ministry of Education, Science and Culture.

REFERENCES

1. D. Ridgly and R. Ward, *J. Am. Chem. Soc.* **77,** 6132 (1955).
2. E. J. Hubibregtse, D. B. Barker, and G. C. Danielson, *Phys. Rev.* **82,** 770 (1951).
3. M. Kestigian and R. Ward, *J. Am. Chem. Soc.* **77,** 6199 (1955).
4. H. P. Rooksby, E. A. D. White, and S. A. Lanston, *J. Am. Ceram. Soc.* **48,** 447 (1965).
5. P. N. Iyer and A. J. Smith, *Acta Crystallogr.* **23,** 740 (1967).
6. M. Abe and K. Uchino, *Mater. Res. Bull.* **9,** 147 (1974).

7. J. B. MacChesney and H. A. Sauer, *J. Am. Ceram. Soc.* **45,** 416 (1962).
8. D. W. Johnson, L. E. Cross, and F. A. Hummel, *J. Appl. Phys.* **41,** 2828 (1970).
9. J. Blatt, D. J. Flood, V. Lowe, P. A. Shroeder, and J. E. Cox, *Phys. Rev.* **13,** 395 (1967).
10. G. R. Caskey, D. J. Sellmyer, and L. G. Rubin, *Rev. Sci. Instrum.* **40,** 1280 (1969).
11. R. P. Huebener, *Phys. Rev.* **146,** 490 (1965).
12. F. Izumi, H. Murata, and N. Watanabe, *J. Appl. Crystallogr.* **20,** 411 (1987).
13. F. Izumi, user's manual for RIETAN.
14. D. A. MacLean, H. N. Ng., and J. E. Greedan, *J. Solid State Chem.* **30,** 35 (1979).
15. D. A. MacLean, K. Seto, and J. E. Greedan, *J. Solid State Chem.* **40,** 241 (1981).
16. F. Lichtenberg, D. Widmer, J. G. Bednorz, T. Williams, and A. Reller, *Z. Phys. B Condens. Matter* **82,** 211 (1991).
17. N. F. Mott and E. A. Davis, "Electronic Processes in Non-Crystalline Materials." Clarendon Press, Oxford, 1979.
18. J. B. Goodenough, "Magnetism and the Chemical Bond." Wiley, New York/London, 1963.
19. N. Tsuda *et al.*, "Electronic Conduction in Oxides." Springer–Verlag, Tokyo, 1990.
20. R. P. Huebener, *Solid State Phys.* **27,** 64 (1972).
21. J. M. Ziman, "Electrons and Phonons." Oxford Univ. Press, London, 1967.
22. K. P. Rajeev, G. V. Shivashankar, and A. K. Raychaudhuri, *Solid State Commun.* **79,** 591 (1991).
23. C. F. van Bruggen, H. C. G. Druiven, R. J. Haange, R. A. M. van Woerden, and G. A. Wiegers, *Mater. Res. Bull.* **22,** 1427 (1987).
24. Chemical Society of Japan (Ed.), "Kagaku Binran," 3rd ed. Maruzen, Tokyo, 1984.
25. H. P. R. Frederikse and G. A. Candela, *Phys. Rev.* **147,** 583 (1966).
26. F. E. Senftle and A. N. Thorpe, *Phys. Rev.* **175,** 1144 (1968).
27. C. Kittel, "Introduction to Solid State Physics," 6th ed. Wiley, New York, 1986.
28. D. C. Johnston, *J. Low Temp. Phys.* **25,** 145 (1976).